RSC Publishing Faraday Discussions

Properties of Feshbach and "shape"-resonances in ozone and their role in recombination reaction and anomalous isotope effect

Journal:	*Faraday Discussions*
Manuscript ID	FD-ART-05-2018-000089.R2
Article Type:	Paper
Date Submitted by the Author:	04-Jun-2018
Complete List of Authors:	Teplukhin, Alexander; Marquette University Babikov, Dmitri; Marquette U., Chemistry

Journal Name

ARTICLE

Properties of Feshbach and "shape"-resonances in ozone and their role in recombination reaction and anomalous isotope effect

Received 00th January 20xx,
Accepted 00th January 20xx

DOI: 10.1039/x0xx00000x

www.rsc.org/

Alexander Teplukhin[a] and Dmitri Babikov[a,*]

Computational modelling of recombination reaction that forms ozone requires inclusion of several quantum mechanical effects such as symmetry, zero-point energy, scattering resonances and tunneling. Major elements of theory for rigorous description of this process are reviewed, with emphasis on interpreting the famous anomalous isotope effect due substitutions of ^{18}O. Three reaction pathways, for formation of symmetric and asymmetric isotopologues of ozone, are introduced and a hierarchy of theory levels is outlined. Lower levels of theory are used to account for the effects of symmetry, isotope mass, rotational excitations and vibrational zero-point energy differences. They happen to be equivalent to statistical description of the process and do not show anomalous isotope effects. Properties of scattering resonances should be included at the next level theory, and may finally explain the isotope effect. Shape resonances, trapped behind the centrifugal barrier and populated by tunneling, can be studied by neglecting couplings between the diabatic ro-vibrational states of the system. Inclusion of these couplings enables formation of Feshbach resonances. Accurate calculations using hyper-spherical coordinates are performed to obtain resonance energies, lifetimes and wavefunctions. Differences between shape resonances and Feshbach resonances are emphasized.

I. Introduction

Ozone molecule, O_3, is a great example of small system where multiple quantum mechanical effects play significant, often crucial roles. First of all, the molecule itself is homo-nuclear and symmetric, so, some ro-vibrational states of O_3 are absent due to quantum *symmetry*.[1-4] Next, quantum scattering *resonances* play role of metastable intermediates O_3^* in the process of ozone formation,[5-7] i.e., through energy-transfer mechanism of recombination:

$$O + O_2 \;\Leftrightarrow\; O_3^* \xrightarrow{+M} O_3.$$

Importantly, quantum *tunnelling* is responsible for formation and decay of some of these metastable states, so called "shape" resonances trapped behind the centrifugal barrier.[8] Feshbach-type resonances happen to be even more important for ozone.[9] Such resonances are populated by coupling between quantum channels, and thus represent manifestation of vibrationally *non-adiabatic* quantum effect. Moreover, when rare isotopes of oxygen are involved (say $Q = {}^{18}O$) quantum *zero-point energy* change is known to be relevant to anomalous rates of the isotope exchange reaction:[10-13]

$$Q + O_2 \;\Leftrightarrow\; QO_2^* \;\Leftrightarrow\; QO + O,$$

which takes place on the potential energy surface of O_3. Finally, presence of rare isotope Q leads to formation of both symmetric and asymmetric intermediate species of ozone, such as OQO^* and QOO^*. Stabilization of those by collisions with bath gas, $O_3^* + M$, is a quantum *state-to-state transition* process in which some relaxation pathways are forbidden by symmetry (e.g., in OOO^* and OQO^*), while others may exhibit unknown propensity patterns (e.g., in QOO^*). It was hypothesized in the past that these features of state-to-state transitions may be responsible for mass-independent fractionation effect in ozone.[14,15]

With this wealth of quantum mechanical effects important for O_3, it becomes clear why the ozone-forming reaction still represents a challenge to chemical physics community. It is quite affordable to run classical trajectory calculations for triatomic and tetra-atomic processes, such as $O + O_2$ and $O_3 + M$ collisions, and it has been done.[16,17] Those studies gave some average information about the energy transfer rates and pathways (e.g., vibrational *vs.* rotational quenching), but the most important questions related to isotope effects remained open. Indeed, classical trajectories are insensitive to zero-point energy change, they violate symmetry restrictions for quantized states and state-to-state transitions, and they can't describe formation of scattering resonances by tunnelling.

On the other hand, quantum mechanical description of the entire ozone formation process is notoriously difficult, and at present time is computationally unaffordable. Since all atoms in the process are heavy (e.g., $M = Ar$ is the simplest bath gas in laboratory experiments, or $M = N_2$ in the air) the number of partial scattering waves and the number of rotational channels for O_3 (heavy rotor) would be far beyond of what is typically

[a] Marquette University, Chemistry Department, PO Box 1881, Milwaukee, WI, USA.
* Corresponding author: dmitri.babikov@mu.edu.

included in the inelastic scattering calculations. Moreover, potential energy well of O_3 is rather deep. It supports over 300 vibrational states that should also be included in calculations (each combined with hundreds of rotational states). The number of resultant ro-vibrational coupled-channels would be huge. It should also be stressed that the initial states in ro-vibrational quenching process are scattering resonances at energies above dissociation threshold (rather than bound states), that can dissociate relatively easily in collision with quencher M. So, strictly speaking, the reactive scattering calculations would be needed for $O_3^* + M$ system (rather than standard inelastic scattering calculations).

In recent years there was a considerable progress in theoretical description of several parts of the overall ozone puzzle. For example, temperature dependence of the isotope exchange process in $O + O_2$ collisions was studied using an improved potential energy surface (PES) of ozone.[18-21] Energies and wavefunctions of vibrational states of O_3 up to dissociation threshold, and some scattering resonances above it, were computed and assigned for $J = 0$.[3,4,22] Energies and lifetimes of scattering resonances O_3^* in a broad range of rotational excitations (up to $J = 60$) were computed neglecting the Coriolis coupling terms and employed to construct a model of ozone formation kinetics, including its temperature and pressure dependencies.[23] Mixed quantum/classical theory was developed to treat ro-vibrational quenching and dissociation of O_3^* within dimensionally reduced approach.[24-26]

Recently, we have undertaken an extensive effort to carry out calculations of energies and lifetimes for scattering resonances in singly- and doubly-substituted isotopomers of ozone that includes symmetric OQO and QOQ, and asymmetric QOO and OQQ species, up to $J = 60$. These data permit to determine the effect of resonance properties on ozone formation rates. A series of papers focused on resultant isotope effects will be published elsewhere.[27,28] Here we want to report one methodological development that was found to be very useful in the case of ozone but also is general, so, it could potentially be used for theoretical treatment of other molecules and/or recombination reactions.

In short, the most complete experimental data for ozone isotopomers are available at room temperature.[10] Theoretical prediction of recombination rate coefficients at these conditions requires averaging over large number of rotational excitations, each included with many scattering resonances, some of which may belong to different types, have very different properties and make rather different contributions. Moreover, besides the actual long-lived ro-vibrational states, the results of matrix diagonalization may contain scattering states, and even some unphysical states (artefacts of numerical approach, that is never perfect). Finally, the value of thermal rate coefficient for complex system may not be fully converged. Analysing results of our calculations for ozone we saw all these complications and struggled to interpret the origin of isotope effects, since those are typically small, often comparable to uncertainties of theoretical predictions. We ended up with a hierarchy of approximations, or theory levels that permitted us to increase complexity of the problem by increments and monitor the "evolution" of isotope effects from the simplest theory level to the most complete.

Namely, at 0th level of theory all minor effects due to isotopic substitutions are neglected and only the effect of symmetry is considered. This is non-trivial for ozone formation kinetics, where large factors on the order of ½ should be properly included in seven different places in the formula to account for symmetries of reagents, products and the number of channels for formation and decay of resonances.[27] At the 1st level of theory the effect of isotope masses is studied using the simplest analytic model for scattering resonances. Such description was shown to be equivalent to statistical approach with partition function introduced at the transition state.[27] The 2nd theory level is based on numerical calculations of "shape" resonances for individual diabatic ro-vibrational channels of ozone (using complex absorbing potential).[28] At the 3rd level of theory the couplings between these ro-vibrational states are taken into account, enabling description of Feshbach resonances[28] and interaction of different reaction pathways on the multi-channel PES of ozone. In this paper we focus on properties of "shape" resonances and Feshbach resonances computed for ozone at the 2nd and 3rd theory level. We will also discuss their relative contributions to the recombination rate and their possible role in anomalous isotope effect.

II. Theoretical Approach

II-A. Kinetics

Ozone is formed by addition of O atom to one or the other end of O_2 molecule. The rate of insertion is small and can be safely ignored. Then, each isotopomer has two pathways for formation and decay of the metastable ozone states (scattering resonances). For example, in the case of symmetric and asymmetric isotopomers of singly substituted ozone we have:

$$O + OQ \overset{A}{\rightarrow} OOQ \overset{B}{\leftarrow} O_2 + Q,$$

$$O + QO \overset{S}{\rightarrow} OQO \overset{S}{\leftarrow} OQ + O.$$

Three physically distinguishable reaction pathways can be introduced: A, B and S. These are not entirely independent, since the reagents for A and S are the same, and the products of A and B are the same. On the global potential energy surface these reaction pathways connect three isoergic entrance/exit channels to three isoergic potential wells where the ozone is formed, as shown in Fig. 1. Note that in hyper-spherical coordinates (ρ, θ, φ) the low-amplitude vibrational motion along hyper-radius ρ and hyper-angle φ describe symmetric and asymmetric stretching of a triatomic, respectively, while large amplitude motion along these two coordinates leads to bond breaking/making and connects reaction channels to product wells, as emphasized by Fig. 1. Hyper-angle θ describes bending, that typically does not lead to dissociation of a triatomic. Conveniently, hyper-radius ρ plays the role of reaction coordinate for the process of

recombination. For 3D pictures of ozone PES using hyper-spherical coordinates see Ref. 29-30.

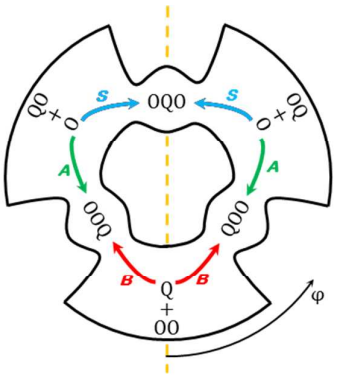

Fig. 1: A map of pathways *A*, *B* and *S* (shown by green, red and blue arrows) for formation of singly substituted ozone. One contour line of the PES is given to show three entrance channels for $O + QO$ and $Q + OO$ reagents, and three wells for symmetric OQO and asymmetric OOQ products. Dashed line represents the reflection plane of

In the steady-state conditions, recombination rate coefficients for these pathways are given by following expressions: [27,28]

$$k^A = \frac{k_{\rm stab}}{q_{\rm O+OQ}} \sum_{J\Lambda p} (2J+1) \sum_i e^{-E_i/kT} \frac{\Gamma_i^A}{\Gamma_i + (k_{\rm stab} + k_{\rm diss})[\rm M]}$$

$$k^B = \frac{k_{\rm stab}}{e^{-\Delta ZPE/kT} q_{\rm Q+O_2}} \sum_{J\Lambda p} (2J+1) \sum_i e^{-E_i/kT} \frac{\Gamma_i^B}{\Gamma_i + (k_{\rm stab} + k_{\rm diss})[\rm M]}$$

$$k^S = \frac{k_{\rm stab}}{q_{\rm O+OQ}} \sum_{J\Lambda p} (2J+1) \sum_i e^{-E_i/kT} \frac{\Gamma_i}{\Gamma_i + (k_{\rm stab} + k_{\rm diss})[\rm M]}$$

In these formula q stands for statistical partition function of reagents, either $O + OQ$ or $Q+O_2$ (including symmetry factor), while ΔZPE is zero-point energy difference of lighter O_2 relative to heavier OQ, as appropriate for channels A, B and S. First summation is over rotational quantum numbers and two parities of symmetric-top functions, second summation is over scattering resonances characterized by energy E_i and decay rate (given by resonance width Γ_i). For asymmetric ozone species OOQ the total decay rate of a resonance is split onto two channels: $\Gamma_i = \Gamma_i^A + \Gamma_i^B$. For simplicity, stabilization and dissociation rate coefficients $k_{\rm stab}$ and $k_{\rm diss}$ are assumed to be the same for all scattering resonances (irrespectively of their rotational and vibrational content or total energy), which is equivalent to strong collision assumption.

II-B. Dynamics

The values of resonance energies E_i and widths Γ_i of O_3 were computed variationally using an efficient approach described in detail elsewhere.[22] It employs hyper-spherical coordinates (ρ, θ, φ) of Parker and Pack[31] with modification of Kendrick,[32] that are perfectly suited to treat three reaction channels on equal footing, and for implementing the symmetries of various isotopomers of ozone. In this approach two-dimensional Schrodinger equation for hyper-angles θ and φ is solved to determine "surface-functions" $\phi_k(\theta,\varphi)$ and their energies ε_k at each point n of ρ-grid:

$$\hat{h}^n \, \phi_k^n(\theta,\varphi) = \varepsilon_k^n \, \phi_k^n(\theta,\varphi),$$

where

$$\hat{h} = -\frac{4\hbar^2}{2\mu\rho^2}\left(\frac{\partial^2}{\partial\theta^2} + \frac{1}{\sin^2\theta}\frac{\partial^2}{\partial\varphi^2}\right) + V(\theta,\varphi)$$

is 2D Hamiltonian operator in the hyper-angles. The effective 2D potential term

$$V(\theta,\varphi) = V_{\rm pot}(\theta,\varphi) + V_{\rm rot}(\theta) - \frac{\hbar^2}{2\mu\rho^2}\left(\frac{1}{4} + \frac{4}{\sin^2 2\theta}\right)$$

includes a 2D-slice of the PES at given point of ρ-grid $V_{\rm pot}(\theta,\varphi) = V(\theta,\varphi;\rho_n)$, and takes into account the effect of rotational excitation within symmetric-top rotor assumption:

$$V_{\rm rot} = \tilde{A}\hbar^2 J(J+1) + (C - \tilde{A})\Lambda^2\hbar^2,$$

i.e., with Coriolis coupling terms and asymmetric-top rotor terms neglected (which is approximation known as centrifugally-sudden, or Λ-conserving, or the coupled-states method).[33-35] $\tilde{A} = (A+B)/2$ is average rotational constant of symmetric top. In the APH coordinates rotational constants are not fixed, they reflect shape of the molecule and depend on θ and ρ as follows:

$$A^{-1} = \mu\rho^2(1 + \sin\theta),$$

$$B^{-1} = 2\mu\rho^2 \sin^2\theta,$$

$$C^{-1} = \mu\rho^2(1 - \sin^2\theta),$$

where

$$\mu = \left(\frac{m_1 m_2 m_3}{m_1 + m_2 + m_3}\right)^{1/2}$$

is a three-body reduced mass of the triatomic.

Surface functions $\phi_k(\theta,\varphi)$ represent locally optimal orthogonal basis sets, at each value of ρ. Their sizes can be reduced individually and efficiently using sequential diagonalization-truncation approach of Bačić and Light,[36] reviewed by Light and Carrington.[37] Then, couplings between different points of ρ-grid, say n and m, are given by elements of the overlap matrix:

$$O_{kl}^{nm} = \langle \, \phi_l^m(\theta,\varphi) | \, \phi_k^n(\theta,\varphi) \, \rangle$$

This information is used to construct the overall Hamiltonian matrix for 3D-problem:

$$H_{kl}^{nm} = O_{kl}^{nm} \times T^{nm} + \delta_{kl} \, \delta_{nm}[\varepsilon_k^n - iU(\rho_n)].$$

Here δ is a Kronecker symbol. Negative complex absorbing potential in the analytic form $U(\rho)$ suggested by Manolopoulos[38] is introduced in the asymptotic range of ρ-grid to convert the scattering problem (above dissociation limit) into the eigenstate problem with complex eigenvalues: $\mathcal{E} = E - i\Gamma/2$. Note that T^{nm} is a matrix of kinetic energy

operator for the remaining third coordinate in the DVR basis, which is a grid of points along ρ. If the grid is equidistant then

$$\hat{T}_\rho = -\frac{\hbar^2}{2\mu}\frac{\partial^2}{\partial\rho^2}$$

Associated volume element in all these equations is trivial: $d\rho d\theta d\varphi$.

For calculations of scattering resonances ρ-grid must extend rather far into the asymptotic region, since it plays the role of reaction coordinate. However, it would be computationally unaffordable to utilize an equidistant grid that, simultaneously, is dense enough (to describe oscillatory behaviour of wavefunction over the deep well) and is long enough (to describe the decay of scattering resonances into the entrance/exit channels). To overcome this problem, an adaptive grid was implemented for ρ with variable step-size optimized to the depth of the PES, based on the value of local de-Broglie wavelength.[39,40] With this approach the kinetic energy operator along ρ is given by:

$$\hat{T}_\xi = -\frac{\hbar^2}{2\mu}\left(\frac{1}{\sqrt{F}}\frac{\partial}{\partial\xi}\frac{1}{F}\frac{\partial}{\partial\xi}\frac{1}{\sqrt{F}}\right)$$

where $F(\xi)$ is Jacobian of transformation between the optimized grid in physical coordinate ρ and an equidistant working grid in the auxiliary coordinate ξ. $F(\xi)$ is determined numerically.[39,40] Each column of the matrix T^{nm} is computed independently using the following steps (as suggested by the equation above): Momentum operator $\partial/\partial\xi$ is applied to the DVR functions divided by $\sqrt{F(\xi)}$, the result is divided by $F(\xi)$, then momentum operator $\partial/\partial\xi$ is applied second time and the result is divided by $-2\mu\sqrt{F(\xi)}/\hbar^2$. Action of the momentum operator $\partial/\partial\xi$ is determined numerically, by forward FFT of the function into the momentum space, followed by multiplication with momenta on the grid and then by backward FFT to the coordinate space.

For completeness, we will mention that two-dimensional solutions $\phi_k\ (\theta,\varphi)$ at each value of ρ-grid were also obtained using sequential diagonalization-truncation method, stating with the FBR of cosine and sine functions for hyper-angle φ, which permits to determine separately 1D solutions $f(\varphi)$ of symmetries A_1 and B_1 (symmetric and antisymmetric, respectively), for each value of θ and ρ. Each set of 1D solutions $f(\varphi)$ was truncated individually and further employed to construct DVR for hyper-angle θ using an equidistant grid in the range $0 \le \theta \le \pi/2$, followed by diagonalization, truncation of 2D basis sets and construction of the DVR for hyper-radius ρ using an optimised grid. Single cut-off criterion was used for all these truncations: $\varepsilon_k < E_{\max}$. The value of $E_{\max}$ was determined by convergence studies. Matrix diagonalizations were done in serial and in parallel, depending on matrix size and computational cost (1D, 2D, 3D) using LAPACK, SCALAPACK and PARPACK packages. The most demanding part of calculations, by far, was construction of the overlap matrix O_{kl}^{nm}, which, however, is amenable to straightforward massive parallelization with negligible message passing.

II-C. Wavefunction analysis

Note that out of three isoergic wells on the global PES of ozone one well holds vibrational states of symmetric OQO, while two other wells hold vibrational states of asymmetric OOQ. So, asymmetric species are represented, effectively, by a double-well potential. This leads to (near) degeneracy of solutions of two symmetries, A_1 and B_1, and basically doubles the number of ro-vibrational states in asymmetric ozone molecules, compared to symmetric molecules. This property is rigorously included into consideration, as it was explained in the Introduction above.[27] Vibrational states of both symmetries A_1 and B_1 are retained for both OOQ and OQO, but are combined with rotational states of opposite parities (and these combinations are made differently for even and odd values of quantum number Λ, see Ref. 27).

In this work, in contrast to other recent papers by our group,[22,23] calculations of vibrational wavefunctions $\phi_k(\theta,\varphi)$ were carried out in the full range of hyper-angle φ used to determine symmetry, which is $0 \le \varphi \le 2\pi$. This permits to describe all isotopologues of the same isotopomer at once. For example, in the case of single substitution, the states of symmetric OQO and asymmetric OOQ are computed simultaneously, in one run. In this way all interactions between the reaction pathways A, B and S during the ozone forming process are also captured by the model.

It should be emphasized, however, that inclusion of all couplings makes calculations more difficult (diagonalization of larger matrixes), but also makes analysis of results rather involved, because all the reaction pathways A, B and S are now linked. Two following tests are needed to analyse wave functions and decay rates of scattering resonances obtained by calculations over three wells on the global PES.

First, the vibrational wavefunction of each resonance must be analysed to determine what product it is associated with, symmetric OQO or asymmetric OOQ? This can be done by integration of probability density through the ranges $120° \le \varphi \le 240°$ and $-120° \le \varphi \le +120°$ that correspond to symmetric and asymmetric species, respectively. Among the long-lived resonances in singly- and doubly-substituted ozone we did not find any states that would mix the wells of symmetric and asymmetric species. Separation between them is usually straightforward. It should be mentioned, though, that in our results we saw quite a few highly delocalized states that describe large-amplitude floppy motion in the van der Waals region of the PES (outside of centrifugal barrier). Those wavefunctions extend through the entire range of the angle φ and describe isomerization between various van der Waals complexes (e.g.: $\mathrm{OQ}\cdots\mathrm{O}$, $\mathrm{QO}\cdots\mathrm{O}$ and $\mathrm{OO}\cdots\mathrm{Q}$ in the singly-substituted case). But, we excluded such states from calculations of recombination rate coefficients, since their stabilization cross-sections are known to be small.[41] At room temperature collision of a van der Waals complex with bath gas M normally leads to dissociation of the complex. Stabilization of van der Waals complex into the covalent well of ozone requires going over centrifugal barrier, through tight transition state, which happens to be a rare event.

Second, the decay rate of each resonance should be split onto the channel-specific decay rates. This is done by integration of resonance wavefunction with absorbing potential placed in one channel at a time. For example, for asymmetric OOQ:

$$\Gamma_i^A/2 = \langle\psi_i(\rho)|U^{\mathrm{O+OQ}}(\rho)|\psi_i(\rho)\rangle,$$

$$\Gamma_i^B/2 = \langle\psi_i(\rho)|U^{\mathrm{OO+Q}}(\rho)|\psi_i(\rho)\rangle.$$

Here $\psi_i(\rho)$ is hyper-radial complex-valued wavefunction of the resonance number i. The value of absorbing potential $U^{\mathrm{O+OQ}}$ is made non-zero only for $60° \le \varphi \le 300°$, while $U^{\mathrm{OO+Q}}$ is non-zero only in the range $-60° \le \varphi \le +60°$. This splitting procedure is checked to ensure that the sum of channel specific decay rates $\Gamma_i^A + \Gamma_i^B$ is equal to the original total decay rate Γ_i obtained by diagonalization of the Hamiltonian matrix, for each resonance. For symmetric species OQO we found that long-lived resonances never decay by releasing the central atom,

$$\mathrm{OQO}^* \;\nleftrightarrow\; \mathrm{OO} + \mathrm{Q},$$

which is consistent with negligibly small rates of ozone formation by insertion in the experiment.[10] Thus, for symmetric species there is no need to split the decay rate. The total value Γ_i is used in calculations of the recombination rate coefficient (see Sec. II-A above).

One more important property of a resonance is probability to find the system inside of centrifugal barrier (at $\rho^\ddagger$), over the well region of the PES, where metastable O_3^* states (scattering resonances) can be efficiently stabilized into stable O_3 molecules by bath gas collisions:

$$p_i^W = \langle\psi_i(\rho)|\psi_i(\rho)\rangle_{\rho<\rho^\ddagger}$$

This property is needed for each resonance because many resonances at higher energies are rather delocalized over ρ and are expected to contribute less to the recombination process (simply because they spend much shorter time over the well region of the PES, $\rho < \rho^\ddagger$, and have smaller chance to be stabilized by bath gas collisions). Ideally, this effect would be contained in the value of stabilization cross section for each resonance (larger stabilization cross sections for localized resonances, and smaller cross sections for delocalized once), but, calculations of stabilization cross sections for individual resonant states are technically unfeasible, as it was outlined in the Introduction. In order to include this effect into our model in a simple way, we compute the value of probability in the well for each resonance and use it to reduce stabilization cross section accordingly, $\sigma_i = \sigma_{\mathrm{stab}} \times p_i^W$. Typical long-lived resonances exhibit $p_i^W \sim 1$ and thus $\sigma_i \sim \sigma_{\mathrm{stab}}$. So, this reduction is important for non-resonant scattering states only, characterized by small probability in the well.

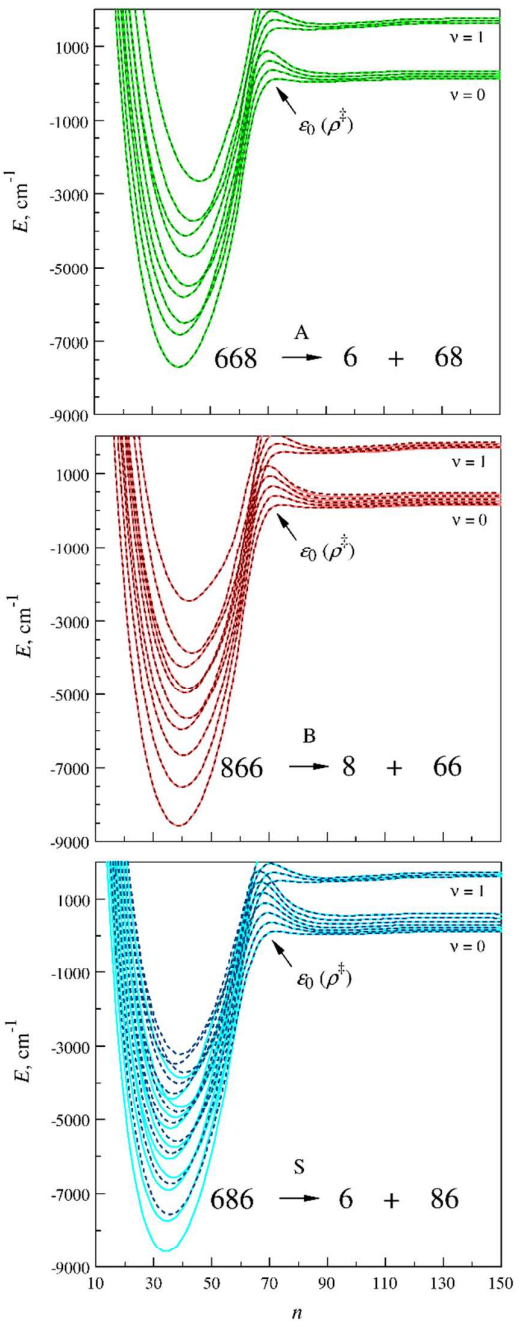

Fig. 2: Energies of diabatic ro-vibrational states computed along the reaction coordinate ρ (grid points are labelled by n) for singly-substituted isotopomer of ozone with typical rotational excitation ($J = 24$, $\Lambda = 8$). Three frames correspond to three channels of ozone formation: *A*, *B* and *S*. Solid and dashed curves correspond to vibrational state symmetries A_1 and B_1, respectively.

II-D. Diabatic Approximations

The goal of symmetric-top approximation discussed in Sec. II-A above is to make calculations affordable by decoupling different Λ-blocks of the Hamiltonian matrix. This is done by neglecting some terms in the Hamiltonian operator (Coriolis couplings and the asymmetric-top rotor terms) to make the matrix block-diagonal. Then, each Λ-block can be diagonalized independently, like if Λ would be a good quantum number. One computational advantage is a lowered memory

requirement, since matrix size is reduced by a factor $J+1$ in each dimension, relative to the fully-coupled calculations. The other, most significant gain, is a reduced cost of matrix diagonalization, that often scales as square or cube of the matrix size. For rotational excitations with $J > 10$ employment of symmetric top approximation becomes critical (recall that for ozone recombination reaction we need to consider up to $J = 60$). Justification for employment of this approximation is that ozone molecule is, indeed, very close to a prolate symmetric top rotor, at least in its equilibrium configuration: $A\hbar^2 = 0.45\ \mathrm{cm}^{-1}$, $B\hbar^2 = 0.66\ \mathrm{cm}^{-1}$ and $C\hbar^2 = 3.56\ \mathrm{cm}^{-1}$.

In this section we will outline two more approximations that are not standard in chemical physics (in contrast to symmetric-top rotor assumption,[33-35] that is known for a long time and is widely used). Our approximations are employed for better understanding of isotope effects in ozone, where the reaction proceeds through several pathways simultaneously. These approximations also appear to be useful for elucidating the role of Feshbach and shape resonances in the recombination process. Computational gain is also substantial (although the question of accuracy should carefully be addressed at some point, see below).

We found that analysis of 2D wave functions $\phi_k(\theta,\varphi)$ in the vicinity of centrifugal barrier (near $\rho{\sim}\rho^{\ddagger}$) permits to split coupled-channels onto three groups that correspond to three reaction pathways: A, B and S. This is easy to do, because at the transition state all wave functions are tightly localized and are found in different sectors of the hyper-angle φ, as one can see from Fig. 1: near $\varphi = \pm 45°$ for pathway B, near $\varphi = \pm 75°$ for pathway A, and near $\varphi = \pm 165°$ for pathway S.

We hoped that it would be possible to completely separate all coupled-channels onto pathways A, B and S, everywhere, through the entire range of ρ. One can start at $\rho{\sim}\rho^{\ddagger}$ and go towards the well region ($\rho < \rho^{\ddagger}$) and towards the asymptotic range of the PES ($\rho \to \infty$), connecting different channels based on values of overlaps O_{kl}^{nm} between 2D-wavefunctions $\phi_k(\theta,\varphi)$ of the adjacent points of ρ-grid. This diabatization method worked, but only partially. Namely, it worked well for several lower energy coupled-channels in pathways A, B and S, where the density of states was not too high. The result of such separation and diabatic connection is shown in three frames of Fig. 2 for pathways A, B and S, respectively, for several lower energy channels of $J = 24$, $\Lambda = 8$. In each pathway symmetric and antisymmetric solutions (of symmetries A_1 and B_1) are shown by solid and dashed lines, respectively. Quick glance over three frames of Fig. 2 tells that different reaction pathways contain different number of diabatic states and exhibit somewhat different well depths. Now we will compare the curves for three pathways in three important regions of the PES: over the covalent well in the range $\rho < \rho^{\ddagger}$, in the vicinity of centrifugal barrier near at $\rho{\sim}\rho^{\ddagger}$, and in the asymptotic range $\rho \to \infty$ (see Fig. 2).

In the well, the diabatic curves for formation of asymmetric OOQ through pathways A and B are nearly degenerate for vibrational solutions of two symmetries (symmetric A_1 and antisymmetric B_1), due to the double-well nature of configuration space occupied by asymmetric species OOQ on the global PES of ozone (see Fig. 1). In contrast, the diabatic curves for formation of symmetric OQO, pathway S, are clearly non-degenerate for symmetries A_1 and B_1, which makes sense for a single-well system.

Near the top of centrifugal barrier all pathways, A, B and S of symmetric and asymmetric species, exhibit (nearly) degenerate vibrational solutions of symmetries A_1 and B_1. This is because, in the entire configuration space $0 \le \varphi \le 2\pi$, each pathway has two energetically equivalent and well separated transition states as one can see from Fig. 1.

In the asymptotic range the diabatic curves for pathway B are non-degenerate for symmetries A_1 and B_1, because there is only one OO + Q entrance/exit channel on the PES. In contrast, pathways A and S connect into two physically equivalent OO + Q entrance/exit channels (see Fig. 1). Therefore, solutions of symmetries A_1 and B_1 are nearly degenerate.

Table 1: Degeneracy of diabatic basis states for three pathways of ozone recombination reaction in three regions of the PES; "deg" means near degenerate solutions of symmetries A_1 and B_1, "non" means non-degenerate solutions of two symmetries.

Recombination pathway	Covalent well	Centrifugal barrier	Asymptotic channels
A	deg.	deg.	deg.
B	deg.	deg.	non
S	non	deg.	deg.

Concise summary of this discussion is given in Table 1, which underlines clearly that there are some fundamental differences between the reaction pathways A, B and S. Moreover, comparing three frames of Fig. 2 one may also notice that the effective well depth for pathway A appears to be shallower than that for pathway B, at least when the diabatic curves for these pathways are decoupled. This is because the ground state function $\phi_k(\theta,\varphi)$, without any excitation quanta, tends to connect diabatically to the pathway B. The next pair of $\phi_k(\theta,\varphi)$ functions, with one quantum of excitation in θ (bending) and in φ (asymmetric stretching), although exhibit similar energies, tend to connect to two different pathways, A and B, respectively. This tendency continues with adding more and more quanta of vibrational excitations in θ and φ, and new diabatic channels connecting to pathways A and B, alternately. However, in the pathway S all these states stay together.

We hoped, initially, to have calculations done for all pathways independently, to find out how these differences translate into recombination rates and, possibly, into the isotope effects. Unfortunately, we were not able to obtain smooth "diabatic" curves for upper ro-vibrational channels (where density of states is higher) needed for convergent results, and, we could not separate pathway A from B in a satisfactory manner, since those two are strongly coupled in the region of the deep well on the PES (which makes sense physically, since these two pathways lead to formation of the same product, asymmetric OOQ). Nevertheless, ro-vibrational

curves for pathways S were easy to separate from the rest, because they couple just to the pathway A (that starts with the same reagents $O + OQ$) and only in the asymptotic region of the PES, where interaction is weak.

In order to do calculations for pathway S independently from pathways A and B it is sufficient to neglect matrix elements O_{kl}^{nm} responsible for this coupling, which effectively splits the Hamiltonian matrix (for each pair of J and Λ values) further onto two blocks. One of those corresponds to the pathway S and can be diagonalized independently to determine energies, widths and wave functions of the corresponding scattering resonances. Note that larger elements of the overlap matrix O_{kl}^{nm} are retained by diabatization of vibrational channels. Neglected matrix elements, those that correspond to the coupling of S to A and B, are typically smaller. Thus, one can hope that this approximation is relatively accurate.

The next approximation we discuss is even cruder, but is also instructive to implement too. In principle, one can try to disregard elements of the overlap matrix O_{kl}^{nm} between different diabatic channels within each pathway (A, B or S). This removes vibrationally "non-adiabatic" couplings and makes every diabatic state independent, described by a small Hamiltonian matrix (size is determined only by the number of points in ρ-grid, which is on the order of two hundred). These small matrixes are very easy to diagonalize independently, for each individual curve of Fig. 2. Note that such wave functions and decay rates do not need to be split between two possible reagents, $O + OQ$ vs. $Q+O_2$, and two possible products, OQO vs. OOQ (e.g., using prescriptions of Sec. II-C), since this is already done but differently, by neglecting the inter-channel couplings in the overlap matrix O_{kl}^{nm}.

What are the goals of these crude assumptions? Neglecting couplings between the diabatic vibrational channels disables mechanism of Feshbach resonances, allowing formation of shape resonances only, populated by tunnelling through centrifugal barrier. The importance, role, and any isotope effects due to shape resonances can be explored in this way. Then, we can include couplings between the diabatic channels, enabling formation of Feshbach resonances (e.g., within pathway S) to explore their role. Finally, the fully-coupled calculations can be done to include interaction between three recombination pathways. Importantly, all three levels of theory are based on the same formalism and the same overall matrix of overlaps O_{kl}^{nm}, but take more and more information from this matrix into account.

III. Results and Discussion

III-A. Shape resonances

Calculations of shape resonances were carried out for rotational excitations in the range $4 \le J \le 56$ and $0 \le \Lambda \le J$, with steps of $\Delta J = 4$ and $\Delta\Lambda = 2$. In each case five lower diabatic ro-vibrational channels of each reaction pathways (A, B and S) were considered, but we found that, typically, only three lower diabatic channels make significant contributions to the recombination rate coefficients, due to fast growth of centrifugal barrier (see Fig. 2) and the effect of Boltzman factor in the formula for rate coefficients (see Sec. II-A). Note that for given Λ the diabatic ro-vibrational states of O_3 correlate asymptotically with ro-vibrational states of O_2 starting at $j = \Lambda$ and going up in j.

Hyper-radial wave function $\psi_i(\rho)$ is presented in Fig. 3 for a typical shape resonance. Over the well region, $\rho < \rho^{\ddagger}$, it describes highly excited vibrational state (ten quanta of vibrational excitation along ρ), while outside of the barrier, $\rho > \rho^{\ddagger}$, it describes a free-moving particle. This particular resonance is located at energy 98 cm^{-1} below the barrier top and has a width of 0.060 cm^{-1}. Overall, we found that the most important shape resonances are located at energies within the range $-200 < \delta E < +300\ cm^{-1}$, where $\delta E = E_i - E^{\ddagger}$ is energy relative to the barrier top determined individually for each diabatic curve (like those in Figs. 2 and 3). At higher energies, widths of these resonances may exceed $10\ cm^{-1}$, but more typical widths are in the range $0.01 < \Gamma < 10\ cm^{-1}$. Narrower resonances are also found (trapped deeper and behind the centrifugal barrier) but their contribution to the recombination process drops quickly as the width is reduced below $\Gamma \sim 10^{-3}\ cm^{-1}$, which corresponds to transition into the so-called high-pressure regime (at experimental conditions of Ref. 10).

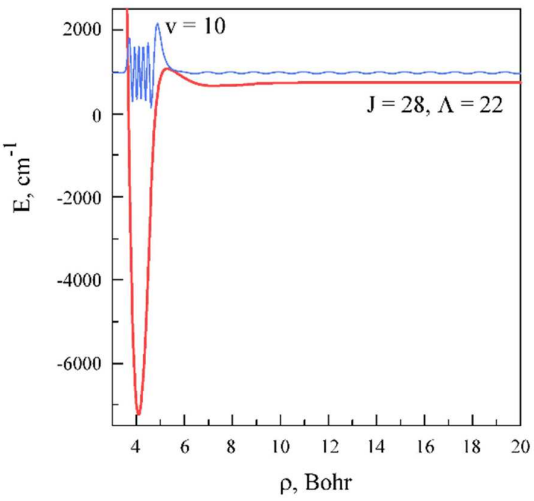

Fig. 3: Hyper-radial wave function of a "shape" resonance in recombination pathway *B* of singly-substituted ozone for rotational excitation $J = 28$, $\Lambda = 22$. Analysis of wave function reveals ten quanta of vibrational excitation along ρ.

In order to analyse and understand the relationship between resonance energies and widths it is convenient to refer to a model, according to which the decay rate (the width Γ) is simply a product of resonance vibration frequency $\tilde{\nu}$ in the well, and the coefficient of transmission through centrifugal barrier.[8,42] For resonances at energies in the vicinity of the barrier top this transmission coefficient can be computed analytically using a model of tunnelling through parabolic barrier.[43,44] Then:

$$\Gamma \approx \frac{\tilde{\nu}}{1+\exp\left\{-2\pi\frac{\delta E}{\hbar\omega}\right\}}$$

where ω is a frequency of parabola that approximates the shape of centrifugal barrier near its top. In the literature, frequency $\tilde{\nu}$ is sometimes set equal to harmonic vibration frequency at the bottom of the well,[42] or computed using classical trajectory,[8] or estimated based on inverse density of states. Neither of these methods is general enough to be used here for prediction of Γ. However, this equation suggests a convenient variable for analysis of resonance properties. Namely, in Fig. 4 we plotted, for all shape resonances computed in this work, the values of their resonance widths Γ_i versus transmission coefficients τ estimated for each resonance individually using its energy δE_i and the barrier shape ω_k of the corresponding diabatic channel:

$$\tau = \frac{1}{1+\exp\left\{-2\pi\frac{\delta E_i}{\hbar\omega_k}\right\}}$$

The value of ω_k varies, depending on rotational excitation J and Λ, roughly from $\omega_0 \sim 100\ \mathrm{cm}^{-1}$ for the ground diabatic state (thicker barrier), and up to $\omega \sim 300\ \mathrm{cm}^{-1}$ for the upper states (thinner barrier). The value of $\tau = 1/2$, that corresponds to a resonance sitting right at the barrier top, is indicated by dashed line in Fig. 4. We see that in a significant range around the barrier top, $0.1 < \tau < 0.9$, majority of computed resonances follow a simple dependence $\Gamma(\tau)$ that can be fitted and used to determine a representative value of $\tilde{\nu}$ for the system.

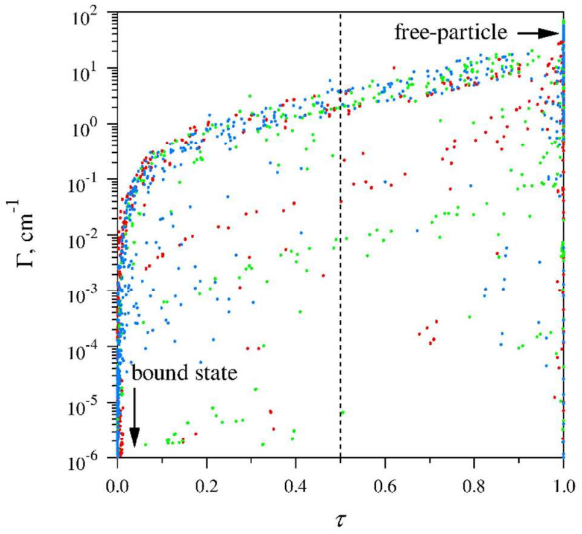

Fig. 4: Resonance width plotted vs. transmission coefficient for shape resonances of singly-substituted ozone molecule in a broad range of rotational excitations. The widths are computed accurately, while transmission coefficients are estimated using a parabolic barrier model. Dashed line corresponds to the top of the barrier. The limits of free-particle and bound states are indicated. See text for details.

Close to 6000 resonances are included in Fig. 4, colour coded by green, red and blue, to distinguish between pathways A, B and S, respectively. In this figure we included resonances at energies below $1000\ \mathrm{cm}^{-1}$ (which is on the order of $5kT$ at room temperature) but we excluded states with negligible probability in the well, $p_i^w < 0.01$ (i.e., scattering states) and states with unphysically large values of width, $\Gamma > \sqrt{2\,\delta E/\mu}/b$, where $b \sim 2$ Bohr is the width of the well that accommodates resonances (i.e., from the repulsive wall at small ρ to the transition state at $\rho^{\ddagger}$, see Fig. 3).

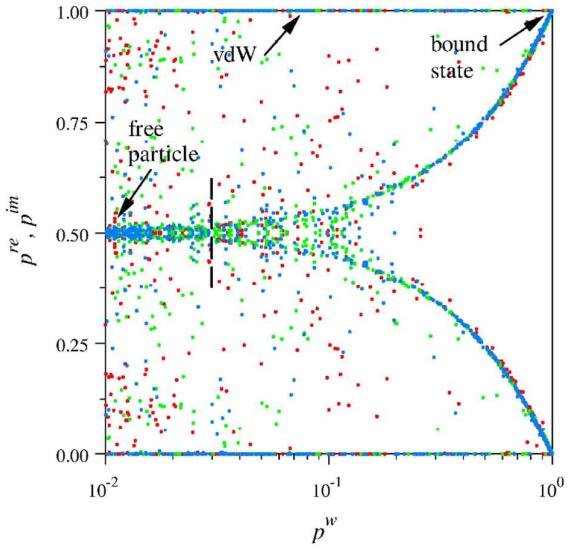

Fig. 5: Same resonances as in Fig. 4 are analysed using probability of finding ozone within the region of covalent well on the PES (horizontal), and two probabilities associated with real and imaginary parts of its wave function (vertical). The limits of bound states and free-particles are indicated. A group of van der Waals states can also be identified.

Besides the main trend in Fig. 4 we also see many points in the range $\tau < 0.1$ where the value of Γ drops much faster (compared to the middle of the interval). These are lower energy resonances trapped deeper in the well, where the barrier shape is not parabolic anymore, but is wider (see, for example, Fig. 2). Tunnelling rates are lower for such resonances, and their widths are much smaller than predicted by the model.

Figure 5 is used to visualize localization of resonance wave functions in the well region. Same six thousand shape resonances as in Fig. 4 are included, and the same colours are used for pathways A, B and S. Horizontal axis gives probability in the well p_i^w as defined in Sec. II-C above, while vertical axis gives probabilities associated with real and imaginary parts of the wave function (i.e., for each individual resonance two dots are plotted at p_i^w, such that the sum of their ordinates p_i^{re} and p_i^{im} is equal to one). Two limiting cases are clearly seen in Fig. 5. One is the limit of a bound state, approached by very narrow resonances that are localized in the well almost entirely ($p_i^w \sim 1$). Their widths are very small, while their wave functions are almost real (so, contribution of the imaginary

part of wave function is close to zero). The opposite limit, approached by short lived scattering states, corresponds to a free particle. Their wavefunctions are highly delocalized (giving small p_i^w) with real and imaginary parts roughly equal to each other. From Fig. 5 we conclude that shape resonances in ozone span the entire range of behaviours, from very narrow nearly bound states, to nearly free-particle scattering states.

In practice it may be helpful to use the point indicated by dashed line in Fig. 5 for separating resonances from non-resonant (scattering) states. Location of such cut-off point is somewhat arbitrary, since it depends on the extent of the grid, or position of complex absorbing potential. In this work, where the grid extends through $\rho^{\max} = 26$ Bohr, the cut-off can be placed near $p_i^w \sim 0.03$ or so, as one can see from Fig. 5.

Figure 5 can also be used to identify van-der-Waals states. Those are found in the van der Waals well, outside of centrifugal barrier, so, they exhibit $p_i^w < 1$. But, many of these states are stable (below the channel threshold), characterized by real-valued wavefunctions. Thus, their corresponding dots appear grouped at the very top (and very bottom) of the graph. The points that spread through the graph in Fig. 5 correspond to mixed resonances that have some probability in the main covalent well, and some probability in the van der Waals well.

Importantly, properties of shape resonances for the reaction pathways A, B and S are all very similar, as one can see from Figs. 4 and 5. Substitution of computed energies E_i, widths Γ_i and well probabilities p_i^w into the kinetics equations of Sec. II-A does not lead to an isotope effect that would look like anomalous isotope effect observed experimentally.[10] This question is discussed in more detail elsewhere[28] and therefore will not be reiterated here. In short, one hypothesis proposed in the past was that tunnelling through centrifugal barrier could be very sensitive to masses of isotopes, which in turn could result in significant differences of properties for shape resonances in pathways A, B and S. But we see opposite. Red, green and blue points in the major part of dependence in Fig. 4 follow the very same trend. Similar, in the major part of dependence in Fig. 5 the red, green and blue points are impossible to tell apart. So, the tunnelling effect, and the shape resonances populated by tunnelling, are unlikely to be responsible for anomalous isotope effect in ozone formation.

III-B. Feshbach resonances

Calculations of Feshbach resonances were carried out for rotational excitations in the range $8 \le J \le 56$ and $0 \le \Lambda \le J$, with steps of $\Delta J = 8$ and $\Delta\Lambda = 8$. In each case 20 coupled channels of each symmetry were included in calculations (for pathway S only, that forms symmetric OQO). It should be mentioned that this number of channels is insufficient for prediction of converged thermal recombination rate coefficient but is enough to see differences between shape resonances and Feshbach resonances.

Two typical Feshbach resonances are analysed in detail in Fig. 6. Upper frame corresponds to a resonance with $\delta E = -38.2\ \mathrm{cm}^{-1}$ and $\Gamma = 0.018\ \mathrm{cm}^{-1}$ $(p^w = 0.92)$ computed for rotational excitation $J = 32$ and $\Lambda = 0$. Lower frame corresponds to another resonance with $\delta E = +70.4\ \mathrm{cm}^{-1}$ and $\Gamma = 0.046\ \mathrm{cm}^{-1}$ $(p^w = 0.94)$ found when $J = 24$ and $\Lambda = 8$. Note that since in these calculations all channels are coupled and participate in formation of a resonance together, it is impossible to assign given resonance to one diabatic channel. So, the value of resonance energy can only be defined relative to the lowest energy barrier, that of the ground state channel in the transition state region (see Fig. 2): $\delta E = E_i - \varepsilon_0(\rho^{\ddagger})$. However, contribution of each channel into a given resonance can easily be determined from computed probability amplitudes a_k of 2D-basis states $\phi_k(\theta, \varphi)$. In Fig. 6 we plotted the values of probabilities $|a_k|^2$ as a function of ρ for four lowest diabatic channels $k = 0, 1, 2$

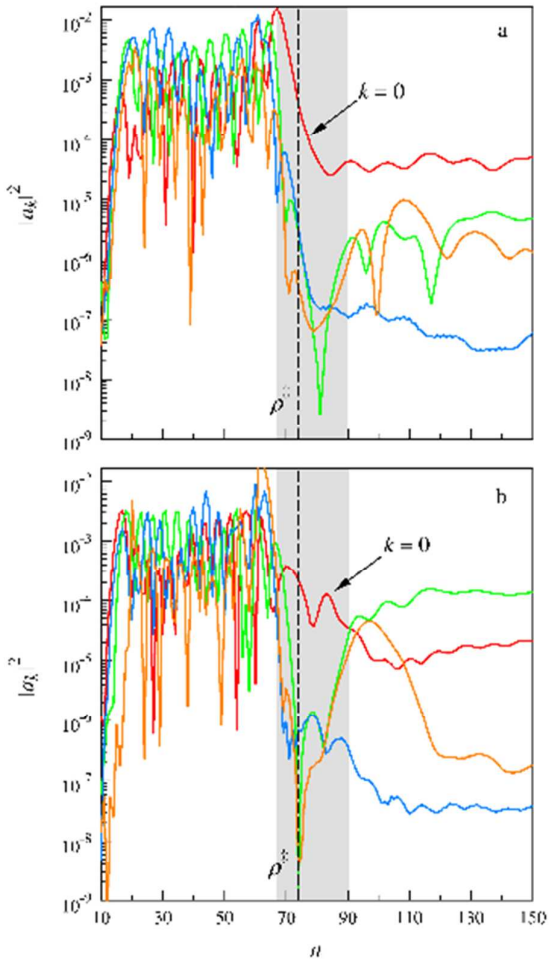

Fig. 6: Contributions of four lower energy diabatic ro-vibrational channels into a typical Feshbach resonance of symmetric singly-substituted ozone molecule OQO. Probabilities for channels $k = 0, 1, 2$ and 3 are shown by red, green, blue and orange colours, respectively. Horizontal axis gives index of grid point along the hyper radial coordinate ρ (just like in Fig. 2). Dashed line indicates position of the barrier top $\rho^{\ddagger}$, grey area is approximately equal to the barrier width. Two different resonances are analysed in the frames (a) and (b). Their parameters are given in the text. Notice that near the barrier all population is restricted to the ground state $k = 0$.

and 3. Position of $\rho^{\ddagger}$ is indicated by dashed line.

From Fig. 6 one can see that in the range of deep covalent well ($\rho < \rho^{\ddagger}$) the four channels are indeed heavily mixed, with somewhat larger contributions of upper states $k = 1$, 2 and 3 and smaller contribution of the ground state $k = 0$. However, in the vicinity of centrifugal barrier (grey area in Fig. 6) contributions of the excited states drop dramatically, by at least four orders of magnitude and even more, while the lowest energy channel $k = 0$ caries almost all probability. Outside of centrifugal barrier ($\rho > \rho^{\ddagger}$), in the asymptotic part of the PES, one of the lower channels may be dominant (e.g., $k = 0$ in Fig. 6a or $k = 1$ in Fig. 6b), or, several channels can mix again.

This observation can be interpreted in the following way. Although Feshbach resonance is formed in the well region of the PES and is populated by couplings between (several, typically many) ro-vibrational channels, still, its wave function should somehow pass through centrifugal barrier. The easiest way for this is to go through the ground state, where the barrier height is smallest, as one can see from Fig. 2. Barriers of the excited ro-vibrational channels are all much higher, because transition state of the ozone PES is relatively tight. Thus, no matter what combination of adiabatic ro-vibrational states is found in the entrance/exit channels of the PES, or over the deep covalent well, we know that in the region of centrifugal barrier the ground state $k = 0$ acts as a gateway.

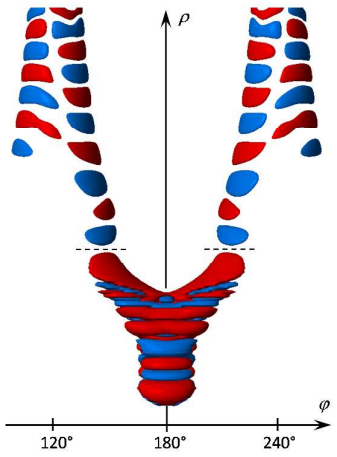

Fig. 7: Three dimensional wave function $\psi(\rho, \theta, \varphi)$ of one Feshbach resonance from Fig. 6. Highly excited vibrational state of OQO can be easily identified in the well region (at the bottom). Leaking of the resonant wave function trough two transition states (dashed lines) into two dissociation channels (at the top) is also seen. The range of ρ is up to 15 Bohr. Transition state is near $\rho^{\ddagger}$ = 5.5 Bohr.

This interesting property may help to develop an approximate model for description of Feshbach resonances in ozone. Three-dimensional wave function for one of resonances in Fig. 6 is presented in Fig. 7. Its shape is rather complicated, but one can identify the "necks" associated with passage of wave function through narrow transition states on the PES. Thus, it may be argued that Feshbach resonances also have to go through centrifugal barrier, but in most cases this is the lowest energy barrier at $\varepsilon_0(\rho^{\ddagger})$. At a model level it should be possible to assume that energies of Feshbach resonances (and the overall number of states) are determined by coupled channels in the potential well, while their lifetimes are still largely affected by passing through centrifugal barrier (of the ground state channel).

In Fig. 8 we summarized properties of Feshbach resonances computed in this work for pathway S of symmetric OQO (roughly two thousand states of two symmetries A_1 and B_1 combined). From this figure we see that many Feshbach resonances go over the barrier of the ground state at $\varepsilon_0(\rho^{\ddagger})$ $\delta E > 0$, although some of them have to tunnel under the barrier ($\delta E < 0$). For those, the value of width Γ drops quickly. Overall, the data points for Feshbach resonances in Fig. 8 show large spread and no particular correlation, in contrast to shape resonances analysed in Fig. 4.

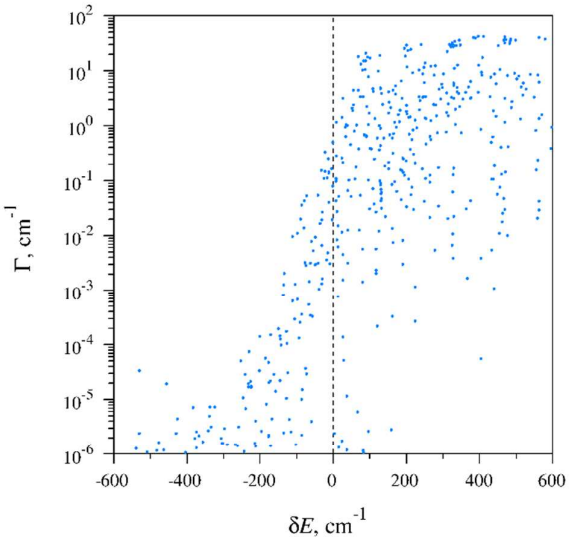

Fig. 8: Resonance width plotted vs. resonance energy δE (relative to the barrier top) for all Feshbach resonances of singly-substituted symmetric ozone molecule OQO (formed through pathway S) in a broad range of rotational excitations, as indicated in the text. Position of the barrier top is indicated by dashed line. Majority of resonances are found above the top and exhibit larger widths, on the order of

IV. Conclusions

In this paper we reviewed several major components of kinetical theory for treatment of ozone recombination reaction with particular emphasis on related isotope effects. When applied to formation of symmetric and asymmetric ozone molecules our approach involves three reaction pathways that connect three entrance channels to three product wells through six transition states. Hyper-spherical coordinates are used to compute energies and lifetimes of scattering resonances, including symmetry restrictions and double-

degeneracies, that describe metastable intermediate states of ozone in the energy-transfer mechanism of recombination.

Diabatic approximation is introduced to define and study shape resonances separately from Feshbach resonances. Properties of shape resonances are easily interpreted based on tunnelling arguments. They can be described reasonably well by a simple analytic model. Feshbach resonances are found to behave differently. Highly mixed in the region of deep covalent well, they basically uncouple in the region of centrifugal barrier and go almost exclusively through one lowest energy channel to reduce or even avoid the necessity of tunnelling. Barrier of the ground state channel is found, typically, at low energy or may even be submerged (when rotational excitation is small). Based on these observations a model may be developed for Feshbach resonances too.

At this point it is hard to come out with predictions or explanations of anomalous large isotope effect observed in the ozone forming reaction. Unfortunately, properties of shape resonances computed and discussed here do not point onto a source of anomalous isotope effect. Calculations of Feshbach resonances with all couplings included between the pathways A, B and S are still in progress. Results presented here were obtained for pathway S only, neglecting its couplings to other pathways, and even those were not entirely converged. We found, however, that contribution of Feshbach resonances into the recombination rate coefficient is much more important than the contribution of shape resonances. So, Feshbach resonances are expected to play dominant role in the process of ozone formation and may indeed hold the key for explanation of anomalous isotope effect.

Conflicts of interest

There are no conflicts to declare.

Acknowledgements

This research was supported by the NSF Atmospheric Chemistry Program, Division of Atmospheric Sciences, grant number AGS-1252486. This research used resources of the National Energy Research Scientific Computing Center, which is supported by the Office of Science of the U.S. Department of Energy under Contract No. DE-AC02-05CH11231.

References

1 D. Babikov, *J. Chem. Phys.*, 2003, **119**, 6554.
2 H. S. Lee, J. C. Light, *J. Chem. Phys.*, 2004, **120**, 5859.
3 D. Lapierre, A. Alijah, R. Kochanov, V. Kokoouline and V. Tyuterev, *Phys. Rev. A*, 2016, **94**, 042514.
4 S. Ndengué, R. Dawes, X.-G. Wang, T. Carrington, Z. Sun and H. Guo, *J. Chem. Phys.*, 2016, **144**, 74302.
5 D. Babikov, B. Kendrick, R. B. Walker, R. T Pack, P. Fleurat-Lesard and R. Schinke, *J. Chem. Phys.*, 2003, **119**, 2577.
6 D. Babikov, B. K. Kendrick, R. B. Walker, R. Schinke and R. T. Pack, *Chem. Phys. Lett.*, 2003, **372**, 686.
7 S. Y. Grebenshchikov and R. Schinke, *J. Chem. Phys.*, 2009, **131**, 181103.
8 D. Babikov, A. Semenov and A. Teplukhin, *Geochem. Cosmo chem. Acta*, 2017, **204**, 388.
9 E. Vetoshkin and D. Babikov, *Phys. Rev. Let.*, 2007, **99**, 138301.
10 C. Janssen, J. Guenther, K. Mauersberger, and D. Krankowsky, *Phys. Chem. Chem. Phys.*, 2001, **3**, 4718.
11 D. Babikov, B. K. Kendrick, R. B. Walker, R. T Pack, P. Fleurat-Lesard and R. Schinke, *J. Chem. Phys.*, 2003, **118**, 6298.
12 R. Schinke, P. Fleurat-Lessard, S. Yu. Grebenshchikov, *Phys. Chem. Chem. Phys.*, 2003, **5**, 1966.
13 R. Schinke and P. Fleurat-Lessard, *J. Chem. Phys.*, 2005, **122**, 094317.
14 D. Babikov, R. B. Walker and R. T Pack, *J. Chem. Phys*., 2002, **117**, 8613.
15 R. T Pack and R. B. Walker, *J. Chem. Phys.*, 2004, **121**, 800.
16 M. V. Ivanov, S. Yu. Grebenshchikov and R. Schinke, *J. Chem. Phys.*, 2004, **120**, 10015.
17 M. Ivanov and R. Schinke, *J. Chem. Phys.*, 2005, **122**, 234318.
18 Y. Li, Z. Sun, B. Jiang, D. Xie, R. Dawes and H. Guo, *J. Chem. Phys.*, 2014, **141**, 81102.
19 Z. Sun, D. Yu, W. Xie, J. Hou, R. Dawes and H. Guo, *J. Chem. Phys.*, 2015, **142**, 174312.
20 T. R. Rao, G. Guillon, S. Mahapatra and P. Honvault, *J. Phys. Chem. Lett.*, 2015, **6**, 633.
21 T. R. Rao, G. Guillon, S. Mahapatra and P. Honvault, *J. Chem. Phys.*, 2015, **142**, 174311.
22 A. Teplukhin and D. Babikov, *J. Chem. Phys.*, 2016, **145**, 114106.
23 A. Teplukhin and D. Babikov, *Phys. Chem. Chem. Phys*., 2016, **18**, 19194.
24 M. V. Ivanov and D. Babikov, *J. Chem. Phys.*, 2012, **136**, 184304.
25 M. V. Ivanov and D. Babikov, *Proc. Natl. Acad. Sci.*, 2013, **110**, 17708.
26 M. V. Ivanov and D. Babikov, *J. Chem. Phys.*, 2016, **144**, 154301.
27 A. Teplukhin and D. Babikov, "Several levels of theory for description of isotope effects in ozone: I. Symmetry effect and Mass effect", *J. Chem. Phys.* (to be submitted).
28 A. Teplukhin and D. Babikov, "Several levels of theory for description of isotope effects in ozone: II. Effect of resonance lifetimes and channel coupling", *J. Chem. Phys.* (to be submitted).
29 M. Ayouz and D. Babikov, *J. Chem. Phys.*, 2013, **138**, 164311.
30 A. Teplukhin and D. Babikov, *J. Chem. Educ.*, 2015, **92**, 305.
31 R. T. Pack and G. A. Parker, *J. Chem. Phys.*, 1987, **87**, 3888.
32 B. Kendrick and R. T. Pack, *J. Chem. Phys.*, 1996, **104**, 7475.
33 R. T Pack, 1974, **60**, 633.
34 P. McGuire and D. J. Kouri, *J. Chem. Phys.*, 1976, **64**, 2488.
35 S. Green, *J. Chem. Phys.*, 1974, **60**, 3463.
36 Z. Bačić and J.C. Light, *J. Chem. Phys.*, 1986, **85**, 4594; J.C. Light and Z. Bačić, *J. Chem. Phys.*, 1987, **87**, 4008; Z. Bačić and J.C. Light, *J. Chem. Phys.*, 1987, **86**, 3065.
37 J. C. Light and T. Carrington, in *Adv. Chem. Phys.*, edited by I. Prigogine and S. A. Rice (John Wiley & Sons, Inc., Hoboken, NJ, USA, 2000), pp. 263–310.
38 D. E. Manolopoulos, *J. Chem. Phys.*, 2002, **117**, 9552.
39 V. Kokoouline, O. Dulieu, R. Kosloff and F. Masnou-Seeuws, *J. Chem. Phys.*, 1999, **110**, 9865.
40 A. G. Borisov, *J. Chem. Phys.*, 2001, **114**, 7770.
41 M. V. Ivanov and D. Babikov, *J. Chem. Phys.*, 2011, **134**, 174308.
42 X. Wang and J. M. Bowman, *Int. J. Quantum Chem.*, 2017, **117**, 139.
43 R. T. Skodje and D. G. Truhlar, *J. Phys. Chem.*, 1981, **85**, 624.
44 L. D. Landau and E. M. Lifshitz, "Quantum Mechanics", 2nd Ed., Pergamon Press, New York, 1965, p. 176.